Undergraduate senior project

Study of cosmic-ray spectrum using gamma-ray data from *Fermi* Large Area Telescope

Patomporn Payoungkhamdee 5705108

Department of Physics, Faculty of Sciences
Mahidol University

"We are trying to prove ourselves wrong as quickly as possible, because only in that way can we find progress."

Richard Feynman

MAHIDOL UNIVERSITY

Abstract

Faculty of Sciences
Department of Physics

Bachelor of Sciences

Study of cosmic-ray spectrum using gamma-ray data from *Fermi* Large Area Telescope

by Patomporn Payoungkhamdee

Cosmic rays (CRs) are high-energy particles propagating in space. They are mainly constituted by protons and the energy spectrum is well described by a power law. Recent measurements by PAMELA and AMS-02 indicate an abrupt change of the CR proton spectral index at about 300 GeV. When protons interact with the Earth's upper atmosphere, γ-rays can be produced and detected by space-based detectors. We use the Earth Limb γ-ray data collected by the *Fermi* Large Area Telescope (LAT) along with proton-air interaction models to determine the CR proton spectral indices that best fit the γ-ray data.

Keyword: Cosmic rays, gamma rays, *Fermi*-LAT

Acknowledgements

I would like to thanks to Dr. Warit Mitthumsiri and Dr. Francesca Spada for their advise and any other supervision.

To begin with project I also appreciate Mr. Suttiwat Madlee for any recommendation and revise my program knowledge. This work also be fulfill the improvement in terms of theory and instrument correction by Prof. Luca Baldini, Dr. Carmelo Sgrò, Mr. Niccolò Di Lalla, Mr. Alberto Manfreda, as well as to people in the Space Physics laboratory at Mahidol University and the Fermi lab at the University of Pisa.

Last but not least, I would like to to thanks Development and Promotion of Science and Technology Talents Project (DPST) for any finalcial support since I was starting this work. This work was partially supported by the Thailand Research Fund award RTA5980003.

Contents

List of Figures

List of Tables

Abbreviations

***Fermi*-LAT** *Fermi* Large Area Telescope 1

PAMELA Payload for Antimatter Matter Exploration and Light-nuclei Astrophysics

CR Cosmic ray 1

γ-ray gamma-ray 1

LRT Likelihood ratio test iv

Physical Constants

Speed of Light	c	=	2.997×10^8 ms$^{-\mathrm{S}}$ (exact)
Mass of proton	m_{p}	=	938.272 MeV/c^2
Mass of Helium atom	m_{He}	=	3.727 GeV/c^2

Symbols

Ω	Solid angle	rad^2
E	Energy	GeV
E_k	Kinetic energy	GeV
R	Rigidity	GV
θ_{LAT}	Azimuth angle from Z-axis of detector plane	rad
ϕ_{LAT}	Angle in +X direction of detector plane	rad
θ_{ZENITH}	Angle between event photon and zenith line	rad
θ_{NADIR}	Defined from inclination angle relative to zenith direction	rad
σ	Crossection	mb

Chapter 1

Introduction

Since the study of Cosmic ray (CR) has been led by Theodor Wulf who taked electrometer measured Cosmic ray (CR) from the ground to higher altitude and much more experiment has confirmed that there is a cosmic ray from outer space which can penetrate to the Earth's surface [1–3].

Consequently, there are many possible phenomena of acceleration mechanism in the space that could produced high energy particles which would be a CR. In order to study the characteristic of acceleration mechanism, we could take consider CR spectrum which has a unique energy break point of superposition between different phenomena.

In 2011, PAMELA detecter indicate that there is a break point of proton cosmic ray spectrum around 240 GV [4]. Furthermore, AMS-02 also found a drastic change of proton CR spectrum at around 336 GV. [5]

CR are mainly compose with proton and 10% by Helium. Generally, gamma-ray (γ-ray) could be produced by CR collide with Earth's upper atmosphere. In this study, we perform an indirect measurement of proton spectrum from γ-ray data which collected by *Fermi* Large Area Telescope (*Fermi*-LAT) to find best fit incident proton spectrum that best fit to γ-ray spectrum.

Chapter 2

Background knowledge

2.1 Cosmic rays

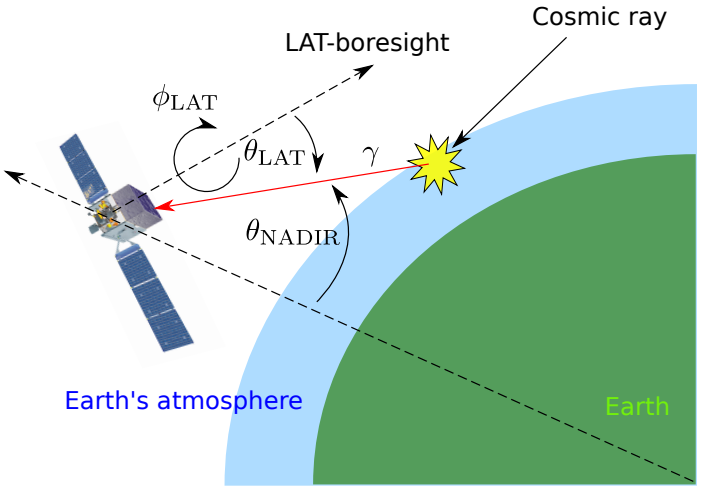

FIGURE 2.1: Schematics of γ-ray production

Cosmic rays are high energic particles which are produced in space by various types of acceleration mechanisms such as supernovae, active galactic nuclei, quasars, and gamma-ray bursts. The main composition of CRs consist of 90% protons, 8% alpha and other heavier atoms. The main reason that makes CRs spectrum follow power law function in rigidity is that the acceleration mechanism process was dominated in Lorenzian interaction which has a characeteristic spectral index.

CR spectrum has various spectral indices at different energies, depending on the types of sources which can accelerate CRs to a certain energy range as shown in Figure 2.1[6].

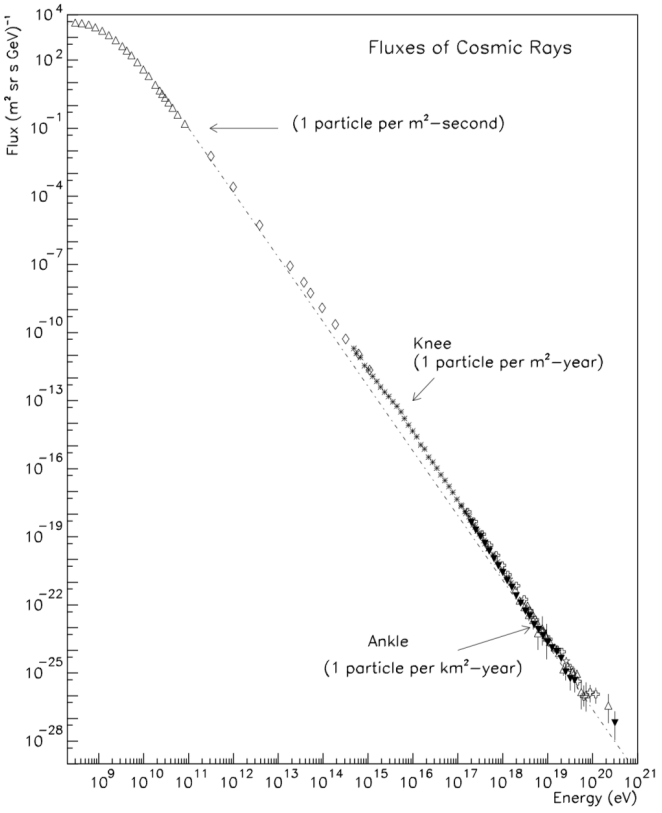

FIGURE 2.2: Main features of cosmic rays spectrum

The motivation why we use γ-ray as a secondary product for investigate incident proton spectrum is that Earth limb's γ-ray relatively brigher than the sky due to collision from CRs in energy range 100 MeV and 1 TeV which consistent with our study [7] as the demonstration in Figure 2.2.

Previous work has been performed using Pass 7 version data [8] and found an energy break point around 300 GeV with a significance of about 2σ [9]. This result is consistent with direct measurements from [4, 5].

2.2 *Fermi* Large Area Telescope

Gamma-ray Large Area Space Telescope (GLAST) could be informally called *Fermi* Large Area Telescope (*Fermi*-LAT). The mission is to collect data of particles from multiple phenomena such as active galaxy nuclei (AGN), pulsars and other high energy sources. It also attach the Gamma-ray Burst Monitor (GBM) to study gamma-ray bursts. Fermi was launched on 11 June 2008 at 16:05 UTC aboard a Delta II 7920-H rocket. Please note that the main content of this section is revised from [10].

2.2.1 Apparatus

LAT consist with 16 layers of traker (TKR) modules, 16 calorimeter (CAL) and a parition ACD.

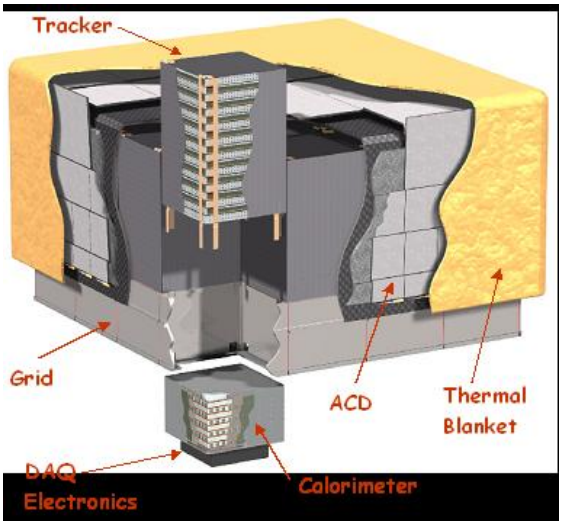

FIGURE 2.3: Instrument structure : Image taken from https://fermi.gsfc.nasa.gov

TKR module has made from an array of silicon-strip tracking detectors (SSDs) and has 18 tracker on a horizontal planes. First 12 planes have 0.035 radiation lengths, next 4 layes contain 0.18 radiation lengths thick and the rest of it does not have any converter. Tracking detector in each plane consist of two planar inner layer which running in x and y axis subsequently. The arrival γ-ray in LAT's field of view could produce electron-positron pair in TKR's plates. The initial lepton pair could be determined from the recoed of conversion point in SSD planes with a power angular resolution when has a low energy.

Each CAL module contains 1536 CsI(Tl) crystal with an 96 crystal align in eight different orthogonal layers. Dual PIN photodiodes also attach in each crystal which provide a great resolution in energy.

ACD tile contain wavelength shifting fiber by photomultiplier tubes (PMT) for redundancy. The tiles also are piled up in one direction.

2.2.2 Event reconstruction

The methodlogy of detection is to track the lepton pair product from an incident photon that collide with a conversion foils and lepton produc be traced by second inner layer of TKR. Consequently, the limit of precision depends on energy of photon that larger than mass energy of electron-positron as well as angle resolution of TKR that getting worser and worser at larger θ_{LAT}. Lastly, the lepton product could be measured the energy by a high precision crystal array in CAL. The event classification also divided into various level of confident event reconstruction with a different Instrument respondse function [11, 12].

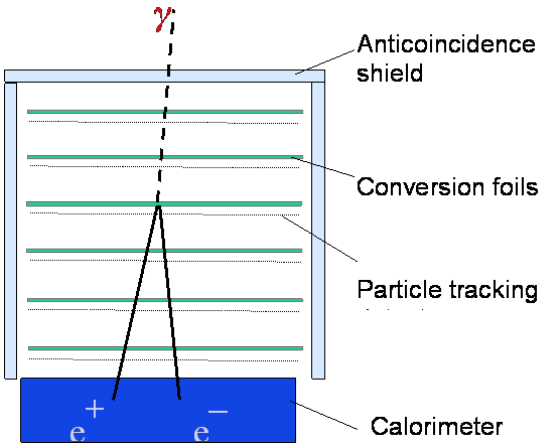

FIGURE 2.4: Schematic Structure of the LAT : Image taken from https://fermi.gsfc.nasa.gov

Chapter 3

Methodology

3.1 Data sets

We use only photon data with a newest version of events reconstruction (would be last version) from *Fermi*-LAT

- P8R2_ULTRACLEANVETO_V6 data from 07/08/2008 to 28/01/2015 ($\sim$7 years)
- Collect photon energy range = 10 GeV to 1 TeV
- $\theta_{\mathrm{NADIR}} = 68.4^{\circ} - 70^{\circ}$(Earth's limb)
- Use $\theta_{\mathrm{LAT}} < 70^{\circ}$

Note that the reasons that we use ULTRACLEANVETO type of event reconstruction are it is the cleanest reconstruction catalogue and uniform distribution of photon in the upper sky which we would use it as a background subtraction.

3.2 Flux extraction

1. Reprocess photon data by taking into account
    - Treat photon energy bias 3.7% that be affected the energy range above 10 GeV
    - Adjust limb angle due to LAT altitude shift due to detection of θ_{Limb} was tilt relatively to altitude of the spacecraft when orbit around asymmetric spherical Earth

2. Construct 2D histogram in Earth's angular coordinate (θ_{ZENITH} and ϕ_{EARTH})

3. Fill photon data in different energy range

4. Calculate exposure maps which include effctive area and time that LAT field of view can glimpse area of interest

5. Divide every single grid count map by exposure map

6. Sum over limb region of this map then divided by solidangle and energy bin width, then fill data in γ-ray energy spectrum as the formula 3.1

$$\text{Flux} \equiv \frac{dF}{dE} = \frac{\int_{\text{Limb region}}(\text{Count map/Exposure map})}{\Delta\Omega\Delta E} \tag{3.1}$$

7. Taking consider background subtraction from a average uniform background photon distribution by treating bin by bin (For more detail see Appexdix A)

3.3 Interaction model

Trail incident proton spectrum in rigidity following relation

Single power law (SPL)

$$\frac{dN}{dR} = R_0 R^{-\gamma} \tag{3.2}$$

Broken power law (BPL)

$$\frac{dN}{dR} = \begin{cases} R_0 R^{-\gamma_1} \ : \ E < E_{\text{Break}} \\ R_0[R(E_{\text{Break}})]^{\gamma_2-\gamma_1} R^{-\gamma_2} \ : \ E \geq E_{\text{Break}} \end{cases} \tag{3.3}$$

Note that power law spectrum in energy has shown in Appendix B.

In this work, we use the scattering amplitude from hadronic collision [13] that could produce a photon particle that could be detected by *Fermi*-LAT.

$$\frac{dN_\gamma}{dE_\gamma} \propto \int_{E_\gamma}^{E_{\max}} dE' \frac{dN_p}{dE'} \frac{d\sigma^{pp\to\gamma}(E', E_\gamma)}{dE_\gamma} \tag{3.4}$$

The atmospheric composition already known well enough that mostly combined with nitrogen gas as well as oxygen molecules [14]. In order to get scattering amplitude from proton-proton collision we treat a crossection of single hadronic collision with a fraction of nitrogen atom which is almost equal to oxygen atom [15] at relativistic level of kinetic energy.

In 2015, the direct measurement of Helium specrtum already reported in [16]. Improvement of model precision was included by taking into account incident of Helium cosmic ray particle as a first order correction and please note that we ignore other heavier atom. The derived equation relation has shown in Eq 3.3 (Derivation has done explicitly in Appendix C)

$$\frac{dN_\gamma}{dE} \propto \sum_{E_{\text{inc,i}}} \left[\frac{E_{\text{inc,i}}}{E_{\gamma,\text{i}}}\Delta(E_{\text{inc,i}})\right]\left[f_{pp}\frac{dN_{\text{H}}}{dE_{\text{inc,i}}}\left\{1+\frac{\sigma_{\text{HeN}}}{\sigma pN}\left(\frac{dN_{\text{H}}}{dR}\right)^{-1}\frac{dN_{\text{He}}}{dR}\frac{dR_{\text{He}}}{dR_{\text{H}}}\right\}\right] \tag{3.5}$$

where

- Red color terms is using for incident proton spectrum that has form like Eq 3.4
- Use helium spectrum from AMS-02 measurement (2015)
- $f_{pp} \equiv E_\gamma(d\sigma^{ij\to\gamma}/dE_\gamma)$ is a table in K&O model which behave like a scattering amplitude that depend on the energy of incident particle
- Crossection $\sigma_{\text{HeN}}/\sigma_{pN}$ at high energy (> 10GeV) is quite stable (≈ 1.6)

3.4 Optimization

Poisson likelihood function define as Eq 3.6

$$\mathcal{L} = \prod_{i=1}^{N} P_{\text{pois}}(n_{\text{i,model}}, n_{\text{i,measurement}}) \tag{3.6}$$

Since our spectrum order is in different decade, we redefined a likelihood as a log-likelihood function for numerically reason like Eq 3.7. In addition,

$$Sum = \sum_{i=1}^{N} -\log P_{\text{pois}}(n_{\text{i,model}}, n_{\text{i,measurement}}) \tag{3.7}$$

In order to get a best fit spectral indices, we do an optimization with a proper trial parameters for take gradient descent from Poisson loss function between model spectrum and flux from measurement as Figure 3.1

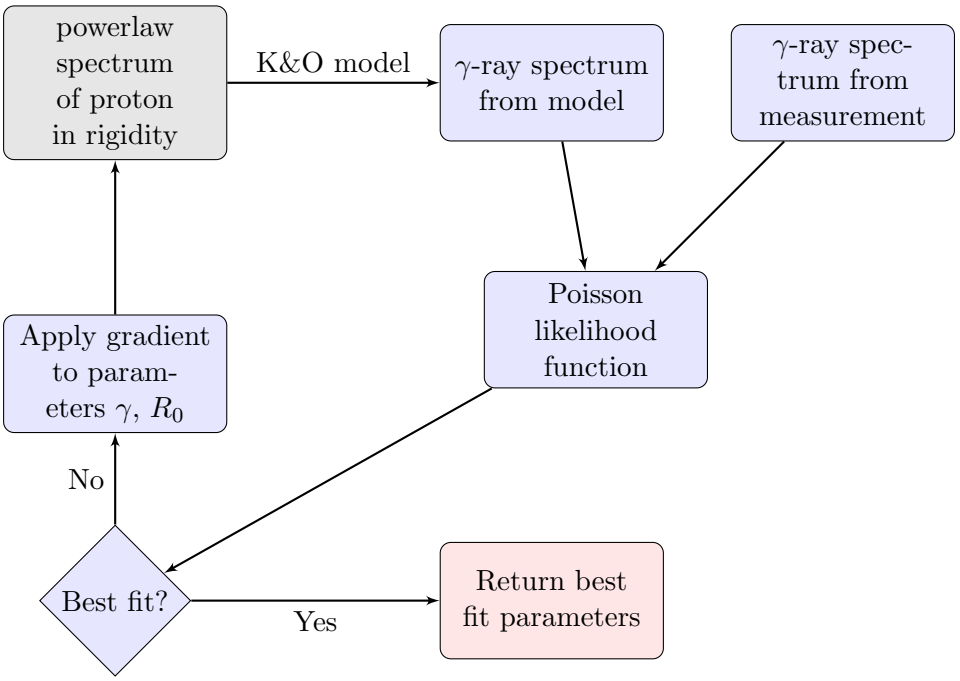

FIGURE 3.1: Flow chart of optimization process

3.5 Monte Carlo Simulation

In this section, we perform a brute force method to find an error of any parameters (spectral indices and break point energy). For a **statistical error (random error)**, we rerandom a counts on each bin by poisson random generator and recalculate the flux after that optimize it as the Fig 3.1 do. The process of this algorithm has shown in Fig 3.2. We do this process as much as gaussian distribution curve looks obvious enough which our work done is roughly 2000 sampling.

For **total error**, we also take into account erro from instrument which is LAT that depends on energy. We exactly the same as the statistical error determination but one more thing that including to this algorithm is to pick three energy bin (10, 100, 1000 GeV) then rerandom flux in these three bin and apply a cubic spline interpolation to smooth the line for a statistical reason [11]. The deminstration of this program is shown as Fig 3.3.

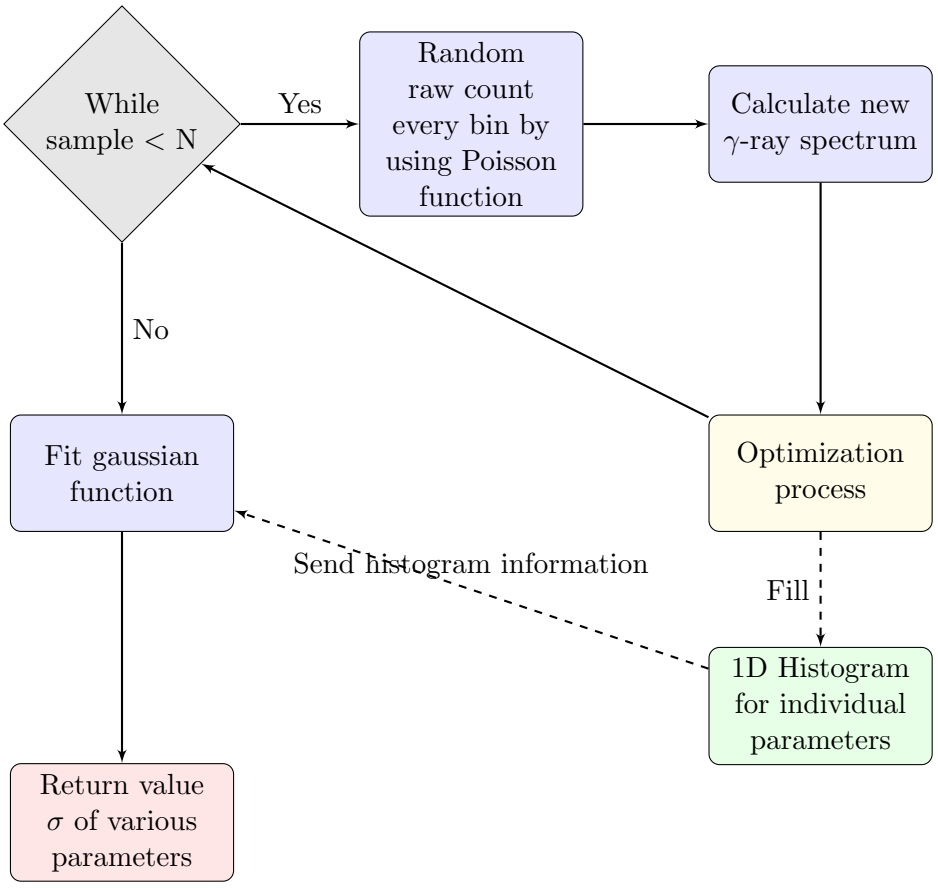

FIGURE 3.2: Flow chart of Monte Carlo simulation for statistical error

3.6 Likelihood ratio test (LRT)

In order to determine significant level between null model and alternative model, we use Wilk's theorem [17]. Basically, this method is to regard a given likelihood

$$\mathcal{L} \equiv \prod_{\alpha=1}^{n} f(x_\alpha, \theta_1, \theta_2, ..., \theta_h) \tag{3.8}$$

where

- x_α is represent a variant from model and data
- θ_i is a degree of freedom (DOF)

The explicit declaration with an obvious method to implement has been proved in [18] as the Equation 3.9

$$\text{LRT} = -2\ln\left(\frac{\mathcal{L}_{\text{null}}}{\mathcal{L}_{\text{alternative}}}\right) \tag{3.9}$$

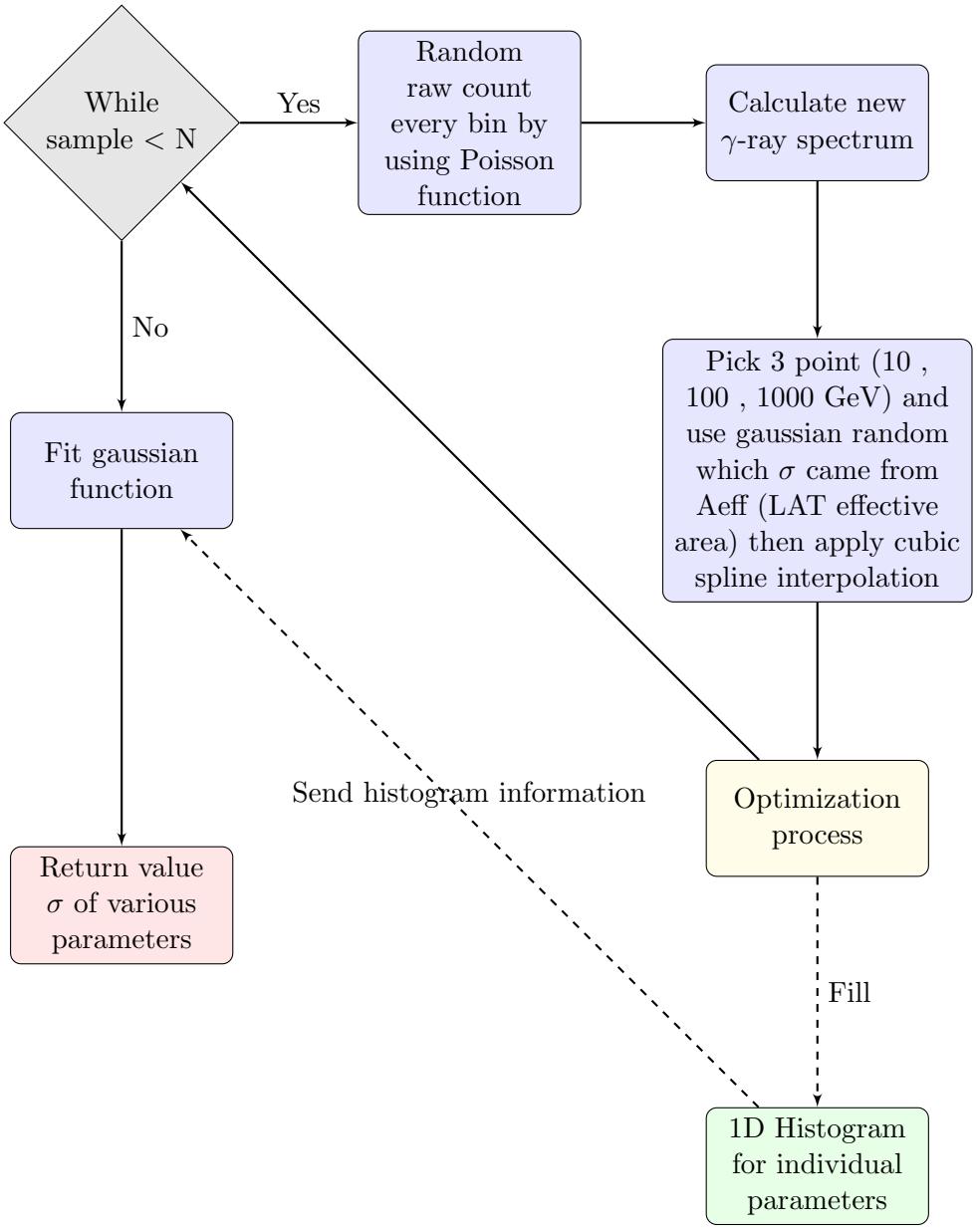

FIGURE 3.3: Flow chart of Monte Carlo simulation for total error

Chapter 4

Results and discussion

4.1 Limb's angle correction

Since we already take into account θ_{ZENITH} shifted due to Earth's radial asymmetry, we should see the count distribution versus θ_{NADIR} with lesser standard deviation as Figure 4.1.

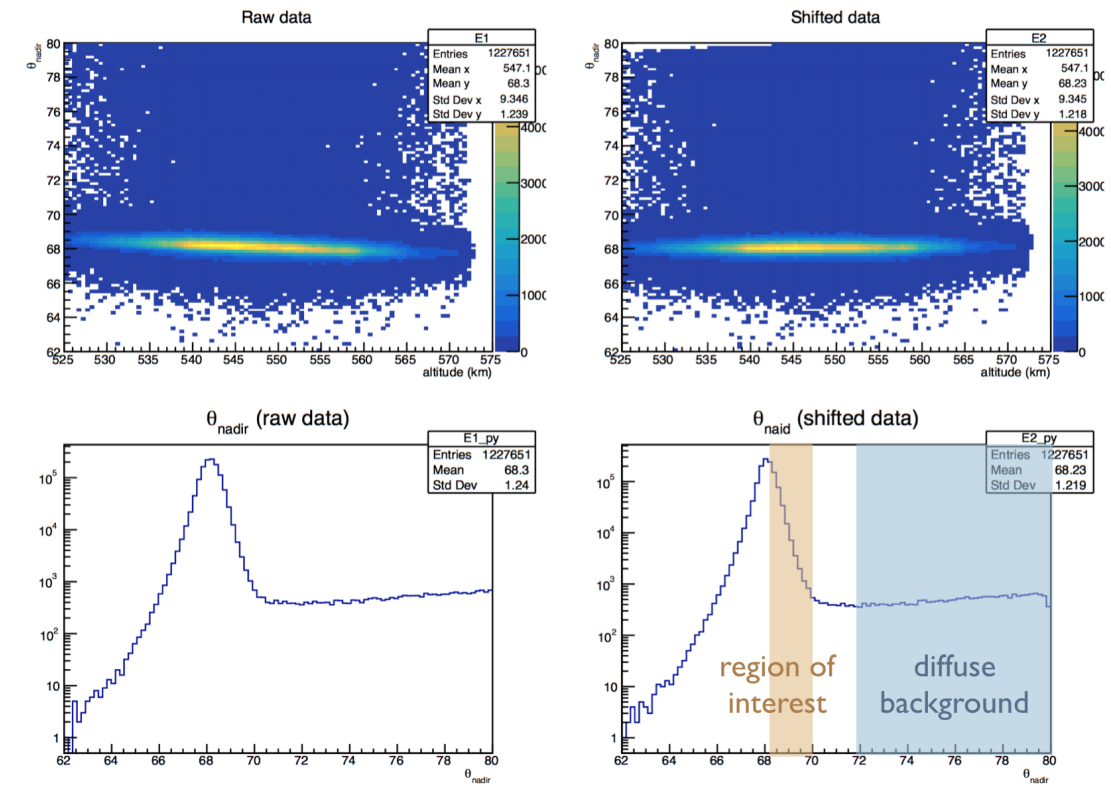

FIGURE 4.1: Distribution of nadir angle before and after altitude correction

4.2 γ-ray spectrum

In this section, we provide an example of various map that we use in Earth's angular coordinate. Please note that we pick only 4 various energy bin to demenstrate by starting with Figure 4.2 for fill a raw event in the map. In order to get an exposure map, we have to dive deep to spacecraft log file to simulate field of view of LAT for count time in each grid on geologic's angular coordinate as well as regard effective area of LAT in different angle as shown in Figure 4.3. Intensity map of photon has a characteristics identification of west and north side like in Fig 4.4, it is obvious to see that west side has higher density than east side because geomagnetic cutoff rigidity when this effect dominated in a lower rigidity. Finally, γ-ray spectrum as in Figure 4.5 could be computed from count map and exposure map with a calculation of Eq (3.1).

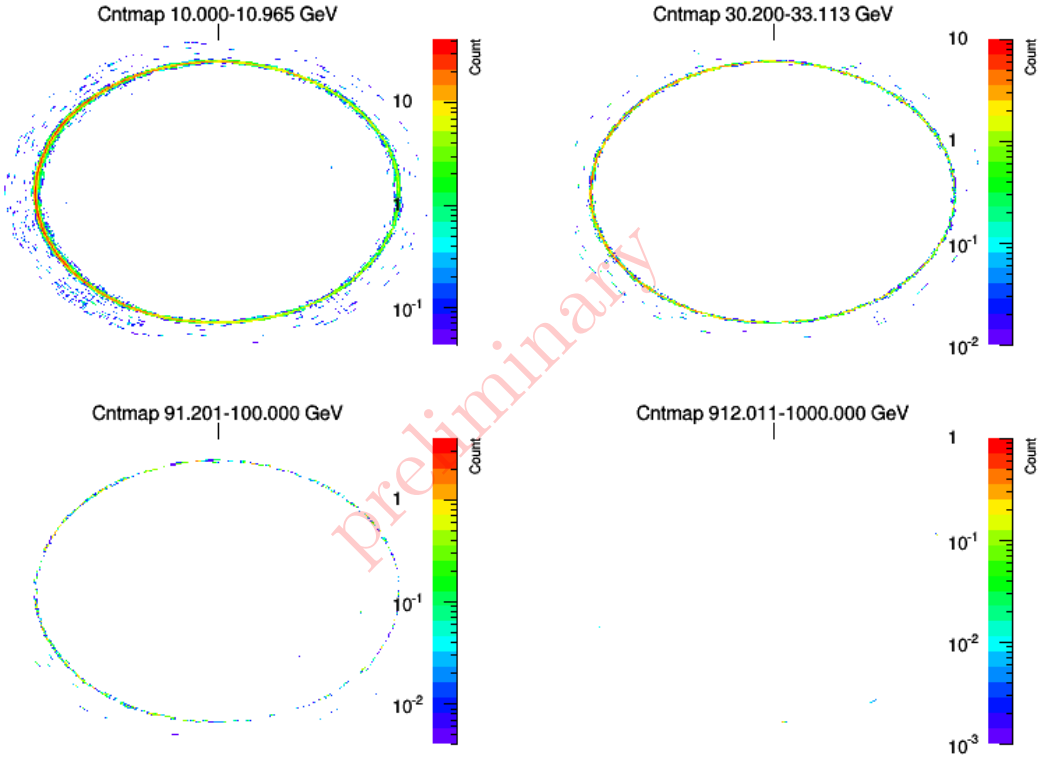

FIGURE 4.2: Count map

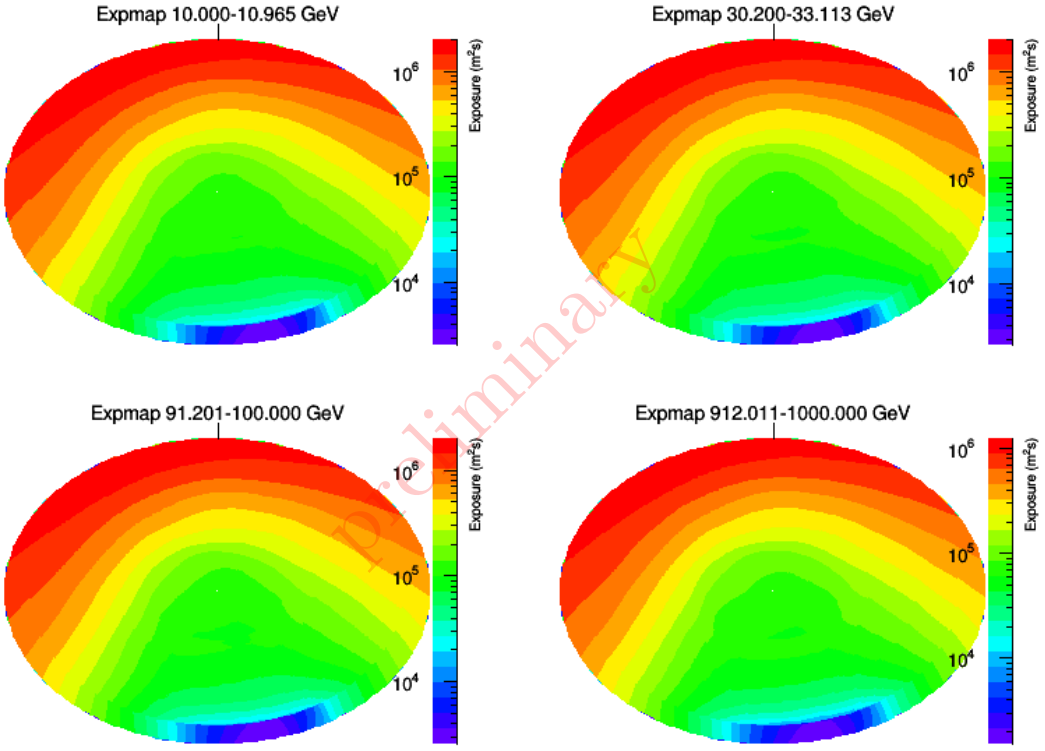

FIGURE 4.3: Exposure map

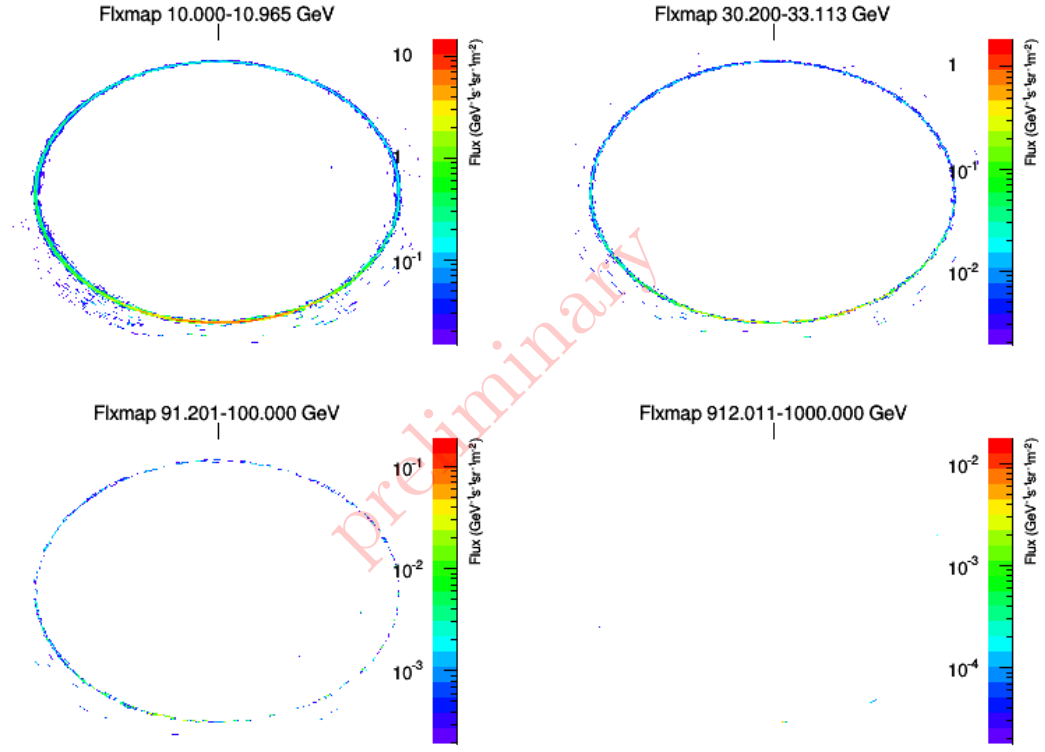

FIGURE 4.4: Flux map

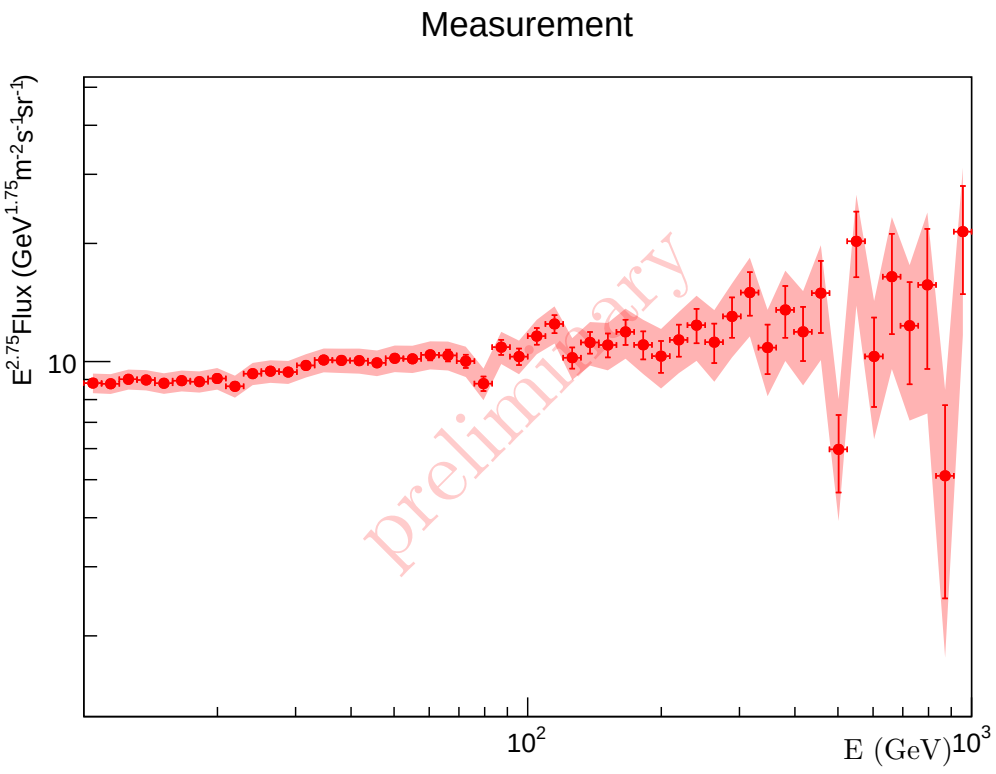

FIGURE 4.5: γ-ray energy spectrum

4.3 Power law from indirect measurement

The measured parameters of SPL and BPL model has been calculated from optimization process has shown in Table 4.1 and we found that BPL fits better than SPL with a significant level of 3.3σ. Note that statistical and total (including systematic error) error computed from Monte Carlo Simulation The demonstration of γ-ray from model and measurement also represent in Figure 4.6 as well as Figure 4.7 show a renormalized proton spectrum from this work (indirect measurement) compare with other direct measurement.

Best fits	γ_1	γ_2	E_{Break} (GeV)
Single Power Law (SPL)	2.68 ± 0.01(0.03)	-	-
Broken Power Law (BPL)	2.84 ± 0.04(0.06)	2.64 ± 0.04(0.17)	328 ± 151(267)

TABLE 4.1: Optimization results :
statistical error and total error has shown in table subsequently

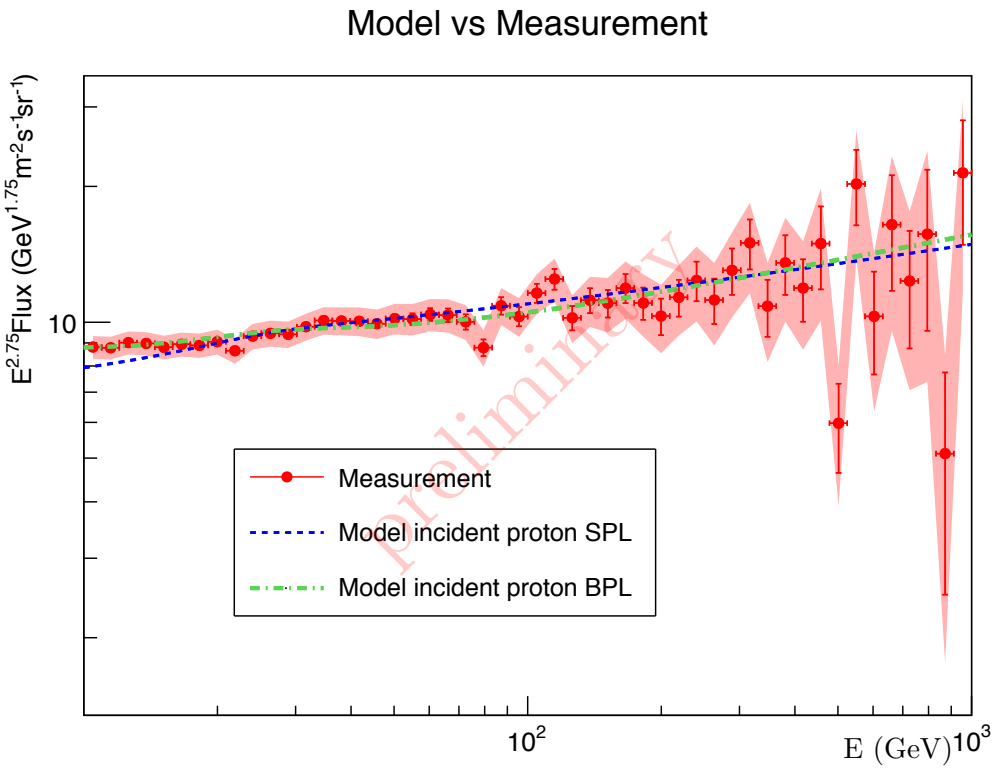

FIGURE 4.6: γ-ray spectrum from model and measurement

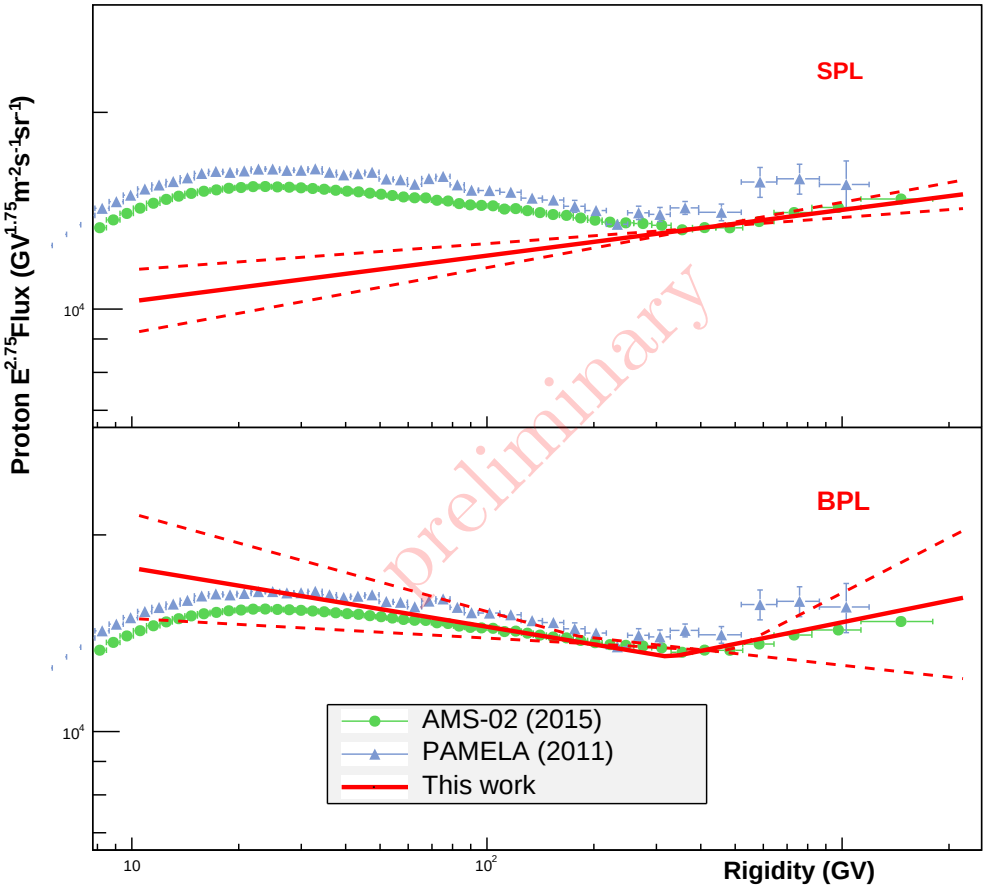

FIGURE 4.7: Proton spectrum from model and other direct measurements

Chapter 5

Conclusion

The result of this work put weight on the previous study [9] that we could take a benefit of brightness γ-ray from Earth's high atmosphere to indirectly observe cosmic ray spectrum which cause this luminous. In this study, we perform an indirect measurement with a newest *Fermi*-LAT's reconstruction event (Pass8) with the same model and modify Helium spectrum by using AMS-02 instead of PAMELA due to it has more precise proton spectrum. To sum up, we found that there is an energy break point around 328 GeV with a significant level of 3.3σ which agree with other direct measurement. Even though we have found better of BPL than SPL, but we still need the significant more than 5σ to strongly comfirm a drastic change of proton spectrum in order of hundren GeV which would be the future work.

Appendix A

Why we can directly subtract a background photon

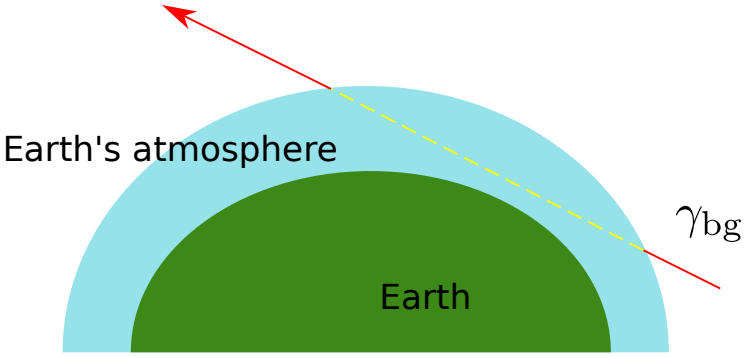

FIGURE A.1: Schematics of γ-ray propagation from diffusive background

Assume Probability of collision with assume ultrarelativistic limit approached to classical concept below

$$N \equiv N_0 e^{-n\sigma x} \tag{A.1}$$

when

- n is a density of air
- σ is a crossection
- x is a propagation length

From using crossection data from XCOM:NIST(2010) [19], we found that collision probability of γ-ray with nitrogen atom and oxygen atom very similar in energy range of our

interest. If we consider in worse case scenario(longest path and highest density that could happen in atmosphere), we found a passing possibility approach to one more than third order. To sum up, we could straightforwardly remove a background by taking average diffusive background per unit of angle before to apply.

Appendix B

Power law in energy

Single power law (SPL)

$$\frac{dN}{dE} = N_0[E_k(E_k + 2m_p)]^{-\gamma/2}\left(\frac{E_k + m_p}{\sqrt{E_k(E_k + 2m_p)}}\right) \tag{B.1}$$

Broken power law (BPL)

$$\frac{dN}{dE} = \begin{cases} N_0[E_k(E_k + 2m_p)]^{-\gamma_1/2}\left(\frac{E_k+m_p}{\sqrt{E_k(E_k+2m_p)}}\right) & : \ E < E_{\text{Break}} \\ N_0[E_b(E_b + 2m_p)]^{(\gamma_2-\gamma_1)/2}[E_k(E_k + 2m_p)]^{-\gamma_2/2}\left(\frac{E_k+m_p}{\sqrt{E_k(E_k+2m_p)}}\right) & \\ : \ E \geq E_{\text{Break}} & \end{cases} \tag{B.2}$$

Appendix C

Derivation of interaction model

Since we know the relation of γ-ray spectrum from incident proton spectrum collide with a nitrogen atom as

$$\frac{dN_\gamma}{dE_\gamma} \propto \int_{E_\gamma}^{E_{\max}} dE' \frac{dN_p}{dE'} \frac{d\sigma^{pN\to\gamma}(E', E_\gamma)}{dE_\gamma} \tag{C.1}$$

Change to discrete form

$$\frac{dN_\gamma}{dE_\gamma} \propto \sum_{E_\gamma}^{E_{\max}} \frac{E_p}{E_\gamma} \Delta(\ln E') E_\gamma \frac{d\sigma^{pN\to\gamma}}{dE_\gamma} \frac{dN_p}{dE'} \tag{C.2}$$

Add first term correction for Helium collision and define $f_{pp} \equiv E_\gamma(d\sigma^{ij\to\gamma}/dE_\gamma)$ which came from K&O model

$$\begin{aligned}\frac{dN_\gamma}{dE_\gamma} &\propto \sum_{E_{\rm CR}=E_\gamma}^{E_{\max}} \frac{E_{\rm CR}}{E_\gamma} \Delta(\ln E_{\rm CR}) \left[E_\gamma \frac{d\sigma^{pN\to\gamma}}{dE_\gamma} \left(\frac{dN_p}{dE_{\rm CR}} \right) + E_\gamma \frac{d\sigma^{HeN\to\gamma}}{dE_\gamma} \left(\frac{dN_{He}}{dE_{\rm CR}} \right) \right] \\ &\propto \sum_{E_{\rm CR}=E_\gamma}^{E_{\max}} \left[\frac{E_{\rm CR}}{E_\gamma} \Delta(\ln E_{\rm CR}) \right] \left[f_{pp} \frac{dN_H}{dE} \left\{ 1 + \frac{\sigma_{\rm HeN}}{\sigma_{\rm pN}} \left(\frac{dN_{\rm H}}{dR} \right)^{-1} \frac{dN_{\rm He}}{dR} \frac{dR_{\rm He}}{dR_H} \right\} \right]\end{aligned} \tag{C.3}$$

In our case, we use the fraction relation of crossection between different atom number with a limit of relativistics as [15], we have found $\sigma_{\rm HeN}/\sigma_{\rm pN} \approx 1.77$

Lastly, term $dR_{\rm He}/dR_{\rm H} = 4$ because the relativistic energy mass relation fraction of rigidity between Helium that approximately heavier than proton 4 times.

Bibliography

[1] V. F. Hess (The Nobel Foundation, 1936).

[2] D. Pacini, Il Nuovo Cimento **3**, 93 (1912), URL https://doi.org/10.1007/BF02957440.

[3] J. Clay, Proceedings of the Section of Sciences, Koninklijke Akademie van Wetenschappen te Amsterdam **30**, 1115 (1927).

[4] O. Adriani, G. C. Barbarino, G. A. Bazilevskaya, R. Bellotti, M. Boezio, E. A. Bogomolov, M. Bongi, V. Bonvicini, S. Borisov, S. Bottai, et al., The Astrophysical Journal **765**, 91 (2013), URL http://stacks.iop.org/0004-637X/765/i=2/a=91.

[5] M. Aguilar (AMS Collaboration), Phys. Rev. Lett. **114**, 171103 (2015), URL https://link.aps.org/doi/10.1103/PhysRevLett.114.171103.

[6] S. Swordy, Space Science Reviews **99**, 85 (2001), ISSN 1572-9672, URL https://doi.org/10.1023/A:1013828611730.

[7] A. A. Abdo, M. Ackermann, M. Ajello, W. B. Atwood, L. Baldini, J. Ballet, G. Barbiellini, D. Bastieri, B. M. Baughman, K. Bechtol, et al. (Fermi-LAT Collaboration), Phys. Rev. D **80**, 122004 (2009), URL https://link.aps.org/doi/10.1103/PhysRevD.80.122004.

[8] M. Ackermann, M. Ajello, A. Albert, A. Allafort, W. B. Atwood, M. Axelsson, L. Baldini, J. Ballet, G. Barbiellini, D. Bastieri, et al., The Astrophysical Journal Supplement Series **203**, 4 (2012), URL http://stacks.iop.org/0067-0049/203/i=1/a=4.

[9] M. Ackermann, M. Ajello, A. Albert, A. Allafort, L. Baldini, G. Barbiellini, D. Bastieri, K. Bechtol, R. Bellazzini, R. D. Blandford, et al. (Fermi LAT Collaboration), Phys. Rev. Lett. **112**, 151103 (2014), URL https://link.aps.org/doi/10.1103/PhysRevLett.112.151103.

[10] *Overview of the lat*, (accessed: 07.06.2018), URL https://fermi.gsfc.nasa.gov/ssc/data/analysis/documentation/Cicerone/Cicerone_Introduction/LAT_overview.html.

[11] M. Ackermann, M. Ajello, A. Albert, A. Allafort, W. B. Atwood, M. Axelsson, L. Baldini, J. Ballet, G. Barbiellini, D. Bastieri, et al., The Astrophysical Journal Supplement Series **203**, 4 (2012), URL http://stacks.iop.org/0067-0049/203/i=1/a=4.

[12] W. Atwood et al. (Fermi-LAT) (2013), 1303.3514, URL http://inspirehep.net/record/1223837/files/arXiv:1303.3514.pdf.

[13] M. Kachelrieß and S. Ostapchenko, Phys. Rev. D **86**, 043004 (2012), URL https://link.aps.org/doi/10.1103/PhysRevD.86.043004.

[14] J. M. Wallace and P. V. Hobbs, *Atmospheric* (Science, 2006).

[15] T. W. Atwater and P. S. Freier, Phys. Rev. Lett. **56**, 1350 (1986), URL https://link.aps.org/doi/10.1103/PhysRevLett.56.1350.

[16] M. Aguilar, D. Aisa, B. Alpat, A. Alvino, G. Ambrosi, K. Andeen, L. Arruda, N. Attig, P. Azzarello, A. Bachlechner, et al. (AMS Collaboration), Phys. Rev. Lett. **115**, 211101 (2015), URL https://link.aps.org/doi/10.1103/PhysRevLett.115.211101.

[17] S. S. Wilks, Ann. Math. Statist. **9**, 60 (1938), URL https://doi.org/10.1214/aoms/1177732360.

[18] J. P. Huelsenbeck and K. A. Crandall, Annual Review of Ecology and Systematics **28**, 437 (1997), https://doi.org/10.1146/annurev.ecolsys.28.1.437, URL https://doi.org/10.1146/annurev.ecolsys.28.1.437.

[19] J. H. M.J. Berger, *Xcom: Photon cross sections database*, (accessed: 07.06.2018), URL https://www.nist.gov/pml/xcom-photon-cross-sections-database.